J. Min. Metall. Sect. B-Metall. 59 (1) (2023) 113 - 123

Journal of Mining and Metallurgy, Section B: Metallurgy

KINETIC MECHANISM OF $FeCr_2O_4$ REDUCTION IN CARBON-CONTAINING IRON MELT

Y.-Y. Xiao [a], L.-J. Wang [a,*], S.-Y. Liu [a], X.-B. He [a], K.-C. Chou [b]

[a] Collaborative Innovation Center of Steel Technology, University of Science and Technology Beijing, Beijing, China

[b] State Key Laboratory of Advanced Metallurgy, University of Science and Technology Beijing, Beijing, China

(Received 15 February 2023; Accepted 04 April 2023)

Abstract

Direct alloying of chromium by chromite attracts a lot of interest for its superiority in energy-saving and process simplification. The knowledge of chromium alloying by reduction of $FeCr_2O_4$, the main component of chromite, is a key to understanding the mechanism of chromium alloying from chromite. The effect of melt composition (carbon and chromium addition) and temperature on the reduction of $FeCr_2O_4$ by carbon-containing iron melt was studied. The higher the carbon content was in the melt, the higher chromium recovery was obtained. Similarly, the higher temperature is favorable for the reduction of $FeCr_2O_4$. The reduction of $FeCr_2O_4$ was impeded by chromium addition due to the lower activity of carbon resulting from the strong attraction between carbon and chromium. The kinetics of $FeCr_2O_4$ reduction by carbon dissolving in iron melt was investigated, and the results indicated that the controlling step was the chemical reaction at the $FeCr_2O_4$/melt interface at 1823K. The calculated activation energy for the chemical reaction was 392.82 kJ/mol.

Keywords: *Chromium alloying; Chromite ore; $FeCr_2O_4$; Stainless steel*

1. Introduction

Chromium is an indispensable alloy element of stainless steel and its addition greatly improves the corrosion resistance of steel. The traditional way to chromium alloy for Cr-bearing steel is the addition of ferrochrome. However, the production of ferrochrome is an intensive energy-consumption process and the recovery ratio of Cr is low. It is produced largely by the submerged arc furnace (SAF) or DC arc furnace. One ton of ferrochrome production in SAF requires 3.5-4.0 MWh of electric energy [1], around 500 kg of coke and 300 kg of quartz, resulting in about 1.2 tons of slag [2]. The high energy consumption needed for ferrochrome production is a burden for Cr-bearing steel production. Moreover, nearly 20% of chromium is lost in slag during the process of ferrochromium production leading to the waste of valuable elements [3-4]. In addition, the production process of iron chromium alloys also produces a large amount of Cr^{6+} containing slag that can cause environmental problems [5].

To reduce electric energy consumption and eventually reduce the cost of Cr-containing steel, a direct alloy technology of smelting reduction has been proposed [6-11]. In this proposed process, the chromite ore or even Cr-bearing slag is introduced to high carbon melt, the reducible oxides are instantly reduced and the valuable elements like iron and chromium are directly dissolved in the melt, that is, the chromium can be directly alloyed into steel. The proposed direct chromium alloying method has the advantages of saving energy and highly integrated production flow which has raised the interest of many researchers.

Carbothermic is a widely used technology to recovery metal from oxides [10, 12]. The recovery ratio of Cr of direct alloying can be improved by pre-reduction through carbothermic reduction of chromite. Many investigations paid close attention to the carbothermic reduction of chromite and elaborate on the characteristic of chromite reduction as discussed in the following, which also enlightened the study of direct alloying of chromium. The main valuable phase in chromite ore was the spinel oxides $FeCr_2O_4$. The reduction sequence of iron and chromium in chromite ore varied in different investigations. It is well known the reduction of iron is ahead of chromium reduction although their reductions overlapped to some degree [13-14], while some researchers [15-16] considered that the reduction of chromium could not happen before the complete reduction of iron. Perry et al. [17] proposed a detailed four stages ion diffusion mechanism of chromite ore reduction: (1) the formation of a slightly

*Corresponding author: lijunwang@ustb.edu.cn

https://doi.org/10.2298/JMMB230215010X

iron-enriched core comprising distorted spinel unit cells surrounded by a region of normal spinel unit cells, affected by the reduction of Fe^{3+} to Fe^{2+} (2) the formation of Cr-Al sesquioxide and Mg-Cr-Al spinel phases effected by the metallization of Fe^{2+} ions and subsequent production of Cr^{2+} ions; (3) reduction of Fe^{2+} interstitials in the spinel core; and (4) metallization of chromium ions via the Cr^{2+} intermediate. Hu et al. [1, 18-20] investigated the effect of iron addition and mill scale addition on chromite ore reduction. The results showed that both iron addition and mill scale were favorable for the reduction of chromite ore by reducing the activity of the reduced chromium.

Although the work on carbothermic reduction of chromite ore is interesting and significant, the practical direct chromium alloying usually happens with the carbon-containing iron melt. The smelting reduction of chromite ore can be split into two processes. One is the dissolution of chromite in slag while the other is the reduction of Cr_2O_3 in slag by carbon-containing melt. Liu et al. contributed to kinetic of chromite dissolution in slag and the kinetic mechanism of the whole reduction process [21-22]. The chromium recovery from the reduction of Cr_2O_3-containing slag by carbon dissolving in the iron melt was also investigated. It was found that the chromite reduction in the slag system involved a stagewise process with an intermediate of divalent chromium [23-24]. Less effort was made to the mechanism of chromite reduction directly in Fe-Cr-C or Fe-Cr-C-Si melt. These works illustrate the effect of flux addition, reduction agent silicon addition, temperature, and rotation speed on chromite reduction by carbon-containing iron melt with the cylinder rotation method [25-28]. The kinetic mechanism of chromite ore reduction was thoroughly studied and the mass transport of oxygen from the concentration boundary layer on the cylinder surface to the iron melt was determined to be the rate-determining step.

In this paper, the reduction of synthetic $FeCr_2O_4$ by carbon in the melt was conducted. The mechanism of chromite reduction in the melt was complicated because it involved the effect of varying reducible components and slag-forming components in chromite. It would be clearer to investigate the chromium recovery in melt without the interference of slag-forming components. Therefore, the investigation of the reduction of pure $FeCr_2O_4$, the main component in chromite, may make an in-depth understanding of direct chromium allying of steel by simplifying the reduction process.

2. Experiment

2.1. Materials

The analytically pure iron powder, Cr_2O_3 powder, and Fe_2O_3 powder (all produced by Sinopharm) were used to synthesize $FeCr_2O_4$ according to reaction (1). The Gibbs free energy of reaction (1) was negative when the temperature ranged from 773K to 1773K, as shown in Fig.1, indicating that reaction (1) was thermodynamically spontaneous. At first, the stoichiometric proportions of Cr_2O_3 powder and Fe_2O_3 powder were well-mixed by a ball mill under 300 r/min for 20 hours. Then the stoichiometric iron powder was added to the well-mixed Fe_2O_3-Cr_2O_3 powder to mix uniformly. An iron crucible containing the last well-mixed Fe_2O_3-Cr_2O_3-Fe powder was put in a graphite crucible which was placed in a vertical resistance furnace. The furnace was heated up to 1373 K under a 100 ml/min argon gas protection and maintained at 1373 K for 24 hours before it was quenched in the furnace. The synthesized $FeCr_2O_4$ was characterized by an X-Ray diffraction spectrum. The XRD pattern of synthesized $FeCr_2O_4$ is shown in Fig.2. The characteristic peaks at 30.147°, 35.509°, 57.070°, and 62.63° were consistent with that of $FeCr_2O_4$ (PDF card no. 34-0140). It indicated that the product was pure $FeCr_2O_4$ without other impurities.

$$Fe(s) + Fe_2O_3(s) + 3Cr_2O_3(s) \rightarrow 3FeCr_2O_4(s) \quad (1)$$

The obtained $FeCr_2O_4$ powder was formed into a dry cylinder without binder by axial pressing in a steel mold under a pressure of 20 MPa maintained for 5

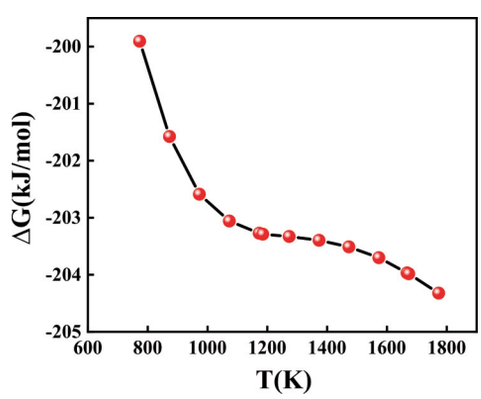

Figure 1. *Gibbs free energy of reaction (1)*

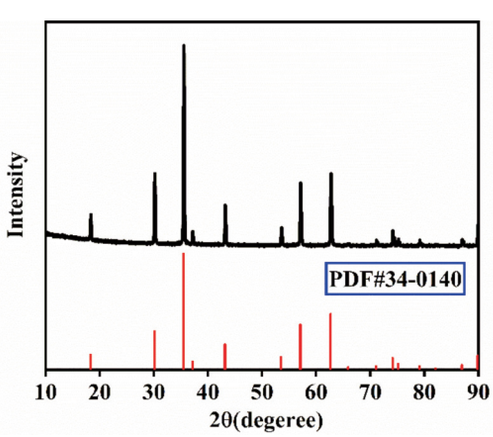

Figure 2. *XRD spectrum of synthetic $FeCr_2O_4$ and standard spectrum of $FeCr_2O_4$*

min. The prepared $FeCr_2O_4$ sample was a cylinder with a bottom diameter of 20 mm and a height of 10 mm. To make sure the cylinder was condensed under experimental temperature, the cylinder was placed in an iron crucible and then heated to 1673 K for 4 hours. Care was taken that the sintered cylinders were free of cracks.

2.2. Experimental procedures

The experiment involved mixing iron powder with a certain amount of graphite or chromium powder, which were all analytically pure and sourced from Sinopharm Group. The mixing process lasted for 20 minutes. The resulting mixture was then melted at a temperature of 1823 K to produce an iron melt with varying levels of carbon and chromium content. The resulting alloy was used for further experimentation.

In a typical experiment, about 150 g (± 1 g) of prepared alloy, as illustrated before, was charged into the φ43mm×50mm×100mm alumina crucible. The alumina crucible was placed in a graphite crucible with the size of φ60mm×70mm×100mm to maintain the reducing atmosphere. The experiment was conducted in a silicon-molybdenum furnace as schematic in Fig. 3. During the whole experiment, the inert gas was charged by the flow of 1L/min measured by a rotary flowmeter. The first sample was taken by a quartz tube with a diameter of 8 mm when the experimental temperature was reached. The first sample was used to obtain the initial [C] or [Cr] content in iron melt. The spinel cylinder (mass was 20 g ± 0.5 g) was charged into the melt which would be semi-immersed in the melt by about 4.5 mm after the first sampling. The time cylinder was charged into the melt and was set to be the start time. Samples were taken at predetermined time intervals of 5, 15, 35, 60, and 90 minutes. The crucible was quenched in water at the end of each run.

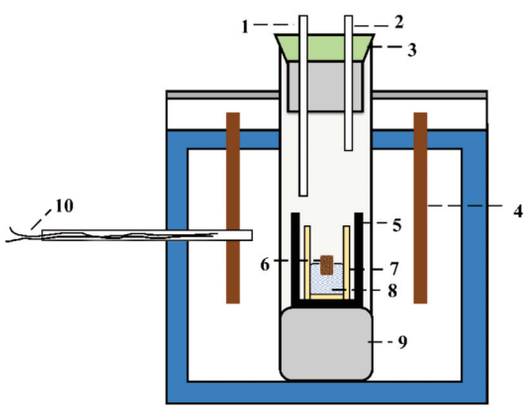

Figure 3. *Schematic diagram of experimental furnace 1. Gas inlet 2. Gas outlet 3. Rubber sealing plug 4. Silicon-Molybdenum heating rod 5. Graphite crucible 6. Charged $FeCr_2O_4$ cylinder 7. Alumina crucible 8. Carbon-containing melt 9. Refractory material 10. Temperature measurement thermocouple*

The influence of melt composition on melt properties was studied by changing the amount of carbon and chromium. The reduction extent Cr(R) was measured in terms of the mass fraction of chromium reduced into the metal phase from the $FeCr_2O_4$ cylinder. The error resulting from the mass of removed samples was corrected. The reduction extent Cr(R) was calculated by equation (2).

$$Cr(R) = \frac{1}{Cr_{FeCr_2O_4}}(Cr_t M_t + \sum Cr_s M_s - Cr_0 M_0) \quad (2)$$

where $Cr_{FeCr_2O_4}$ is the total mass of elemental chromium in the cylinder (g); Cr_t is the mass percentage of chromium in the melt at the time t; Cr_0 is the mass percentage of chromium in the starting melt; Cr_s is the mass percentage of chromium in each of the previous samples; M_s is the mass of each previous sample; M_t is the mass of the melt at time t (g); and M_0 is the initial mass of the melt (g).

2.3. Characterization

The samples obtained were milled into powder and the chromium content of the samples was analyzed by an inductively coupled plasma optical emission spectrometer (Optima 7000DV, PerkinElmer, America). The mass content of carbon in samples was analyzed by a Carbon-Sulfur analyzer (EMA-820V, LECO, Japan). The SEM images and EDS analysis were conducted on SEM-EDS combination equipment (FEI Quanta, Netherland). The XRD analysis was conducted on an X-ray Powder diffractometer (SMARTLAB, Japan Science Corporation, Japan).

3. Results and discussion

3.1. Effect of metal composition

3.1.1. Effect of carbon content

Fig.4 shows the effect of carbon content on the reduction of $FeCr_2O_4$. Fig. 4(a) and (b) represent the Cr(wt%) and C(wt%) in sampled metal, respectively. The more initial carbon content in the melt, the more chromium recovery in 90 min was obtained. When the initial carbon content was 5.18 mass%, 4.81 mass%, and 3.40 mass%, the reduction extent of $FeCr_2O_4$ reached 87.94%, 70.50%, and 47.67%, respectively. The reduction degree with an initial carbon content of 5.18 wt% at 1823 K was better than the 12% of ERIC and his coworkers under carbon saturation conditions at 1873 K. [28] The use of natural chromite as raw material in their experiment may be the reason for the difference. It is found that the reduction rate of $FeCr_2O_4$ increased with the increase of initial carbon content. In general, the slope of the curve decreased

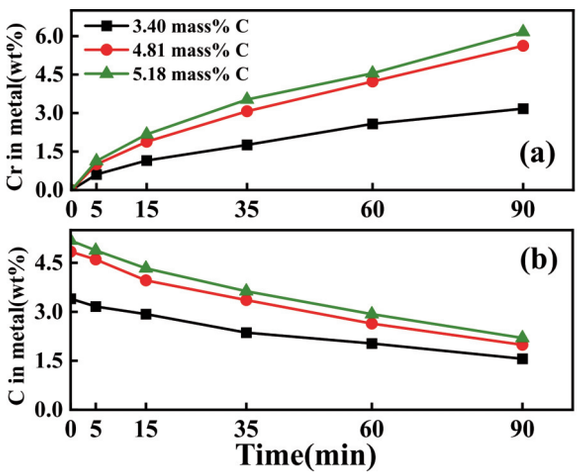

Figure 4. *Content of (a)[Cr] and (b)[C] in iron melt with different initial carbon content at 1823K*

with the progress of the reaction, that is, the reduction rate slowed down with the decrease of carbon content and the increase of chromium content. Accordingly, the decrease of carbon content slowed down as reduction proceeded. This can be explained thermodynamically from the Gibbs free energy of the reduction of $FeCr_2O_4$. The reduction of synthesized $FeCr_2O_4$ in liquid Fe-C is represented by reaction (3). The Gibbs free energy of reaction (3) increased with the decrease of the carbon activity and increase of chromium activity.

$$FeCr_2O_4 + 4[C] \rightarrow Fe(l) + 2[Cr] + 4CO(g)$$
$$\Delta G^{\theta} = 955420 - 602.82T \; J/mol \quad (3)$$

Fig. 5(a) shows the relationship between carbon activity and reduction rate. The x-axis, from the right to the left in each line, is the carbon activity after the reaction for 0, 5, 15, 35, and 60 minutes. The y-axis, from the top to the bottom in each line, is the mass of reduced $FeCr_2O_4$ every minute in the five time periods. There is a linear relationship between carbon activity and reduction rate after the first 5 minutes. This indicated that the chemical reaction was likely to be the rate-controlling step for $FeCr_2O_4$ reduction. The change of slope between carbon activity and reduction rate after 5 minutes may be attributed to that, compared to the condition with chromium addition, the carbon activity decreased more intensely with decreasing carbon content without no chromium addition, as shown in Fig. 5(b). As a result, the slope between carbon activity and reduction rate decreased after 5 minutes.

3.1.2. Effect of chromium addition

The effect of initial chromium content on the increase of chromium content in obtained metal is shown in Fig.6. Fig. 6(a) and (b) represent the increased Cr(wt%) and C(wt%) in sampled metal, respectively. A positive effect of chromium on chromite reduction was reported in some articles explained by the increasing ratio of the initial to final carbon activity with chromium addition [25, 27-28].

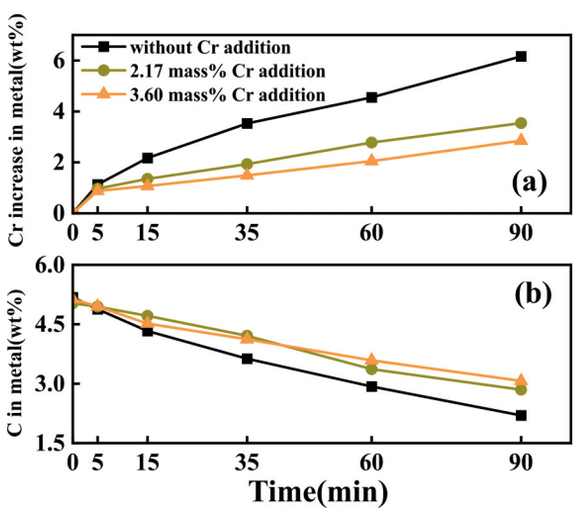

Figure 6. *(a) [Cr] increase and (b) [C] content in iron melt with different initial chromium content at 1823K*

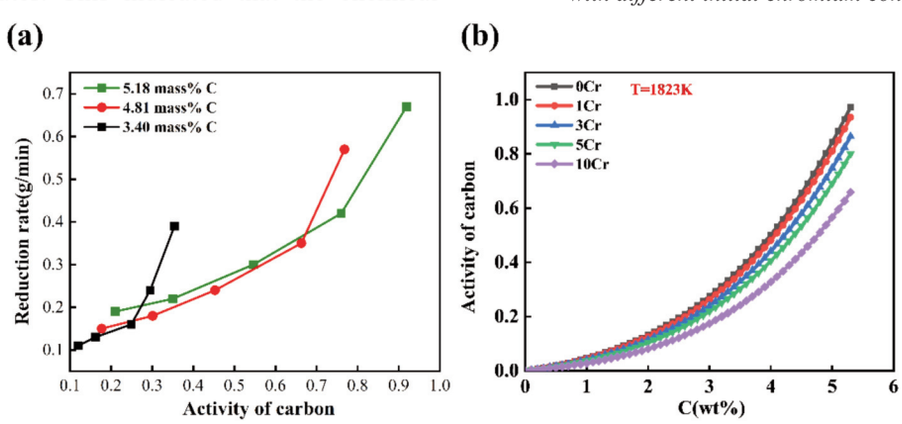

Figure 5. *(a) Relationship between carbon activity and reduction rate of $FeCr_2O_4$ (b) Effect of initial chromium on carbon activity in Fe-C-Cr system*

However, the obtained results from this experiment inferred that chromium recovery decreased with the increase of initial chromium content. On one hand, the chromium addition decreased the carbon activity in the melt, as shown in Fig. 5(b). On the other hand, the chromium addition would increase the reaction quotient which increased the Gibbs free energy of $FeCr_2O_4$ reduction. As a result, the attempt to obtain a higher chromium alloy by increasing initial chromium content in liquid Fe-C-Cr occurred at the cost of reducing chromium recovery. In addition, different from the experiment without chromium addition, the reduction rate was almost unchanged after the first 5 min when chromium was added to the 4 iron melt.

3.1.3. Effect of temperature

Fig.7 shows the effect of temperature on chromium recovery by reduction of $FeCr_2O_4$. These experiments were conducted at different temperatures with initial carbon content of 3.40 wt%. The iron melt was free of chromium at the beginning. Fig. 7(a) shows increased Cr(wt%) with reaction time and Fig.7(b) depicts the C(wt%) in sampled metal. Experimental results suggested higher temperature was favorable for the reduction of $FeCr_2O_4$ by carbon dissolved in iron melt. This occurred because higher temperature favored the decomposition of the oxide and the reduction reaction, both of which were endothermic. Therefore, the higher temperature showed great promotion in chromium recovery. Moreover, the reduction rate increment was more significant when the experiment temperature increased from 1823 K to 1873 K compared to that when the experiment temperature increased from 1773 K to 1823 K.

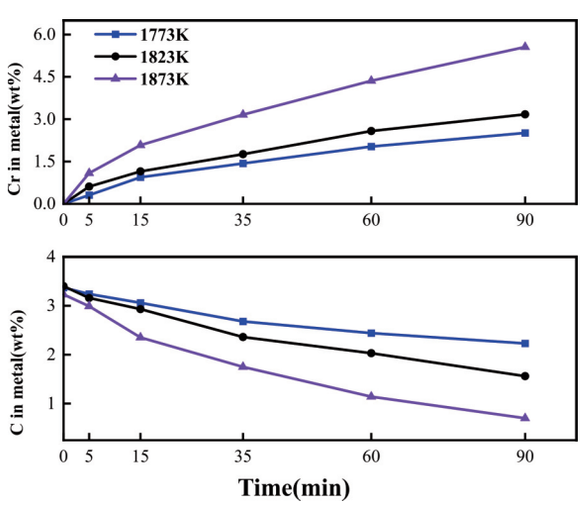

Figure 7. Content of (a)[Cr] and (b)[C] in iron melt at different experiment temperatures

3.2. Kinetic analyses of $FeCr_2O_4$ reduction by carbon in melt

The reduction of $FeCr_2O_4$ by carbon dissolved in iron melt involves the reduction of iron and chromium, as shown in the schematic diagram in Fig.8. It can be divided into elementary steps as following:

1) Dissociation of $FeCr_2O_4$ on the $FeCr_2O_4$-melt interface:

$$FeCr_2O_4(s) \rightarrow 2[Cr] + [Fe] + 4[O] \qquad \Delta G^{\theta} = 967062 - 412.83T \tag{4}$$

2) Transport of chromium, iron, and oxygen from the $FeCr_2O_4$/melt interface to the melt.

3) Transport of the carbon and oxygen from melt to the metal/gas interface and transport of iron and carbon from the iron melt to the $FeCr_2O_4$/melt interface.

4) The reaction of oxygen and carbon at the melt/gas interface to form CO molecule:

$$[C] + [O] \rightarrow CO(g) \qquad \Delta G^{\theta} = -23430 - 39.2T \tag{5}$$

5) Nucleation and escape of CO gas

The Gibbs free energy of $FeCr_2O_4$ dissociation would be less than zero when $a^2_{[cr]}a^4_{[o]}$ was less than 7.16×10^{-7} when the standard state was 1 wt%. According to the study of MATOUSEK [29], the solubility of [O] in iron ranges was about 200 ppm which indicated that the activity of [O] was in the order of 10^{-4}. As a result, the dissociation of $FeCr_2O_4$ was thermodynamically possible. In addition, it is widely accepted that steps (1) and (5) could not be the rate-determining steps due to the high temperature under experimental conditions [25-28]. Given the relatively high equilibrium concentration of Cr in Fe, the mass transport of Cr could be eliminated from the rate-determining step. The mass transfer of carbon was assumed to be fast in the experimental carbon content range [30]. To the best of the researcher's knowledge, there only exists one study in the literature that mentions the mass transfer of carbon

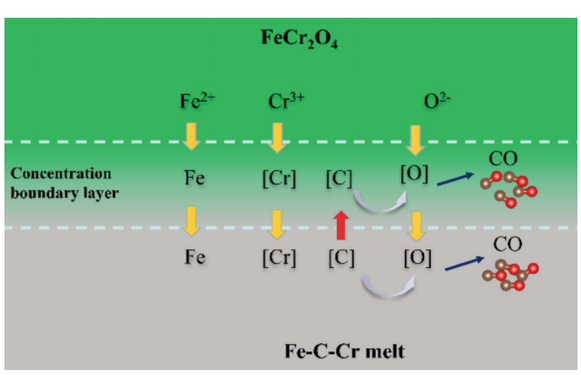

Figure 8. Schematic diagram of $FeCr_2O_4$ reduction in carbon-containing melt

from the melt to the oxide-melt interface is the rate-controlling step, when the carbon content is lower than 0.8 mass%, for the reduction of Cr_2O_3 by carbon dissolving in iron melts [31]. The carbon content in this paper was higher than that indicating the mass transfer of carbon was not likely the rate-controlling step. Many investigators concluded that the CO formation is controlled by a chemical reaction at the interface during the decarburization process of the iron melt containing carbon [32-34]. As a result, the mass transport of oxygen, carbon and reaction for CO formation may be the rate-determining step. To find the rate-determining step of the reduction of $FeCr_2O_4$ under the experimental condition, the kinetic equation assumed that the mass transport of oxygen and CO formation reaction is the rate-determining step will be discussed.

3.2.1. Interfacial reaction

If the reduction of $FeCr_2O_4$ was controlled by the CO formation reaction, the reduction rate of $FeCr_2O_4$ could be expressed as:

$$4\frac{dn_{FeCr_2O_4}}{dt} = \frac{dn_C}{dt} = k_r AC \tag{6}$$

where the k_r is the reaction rate constant. The A and C are the interfacial area and the molar concentration of carbon at the interface, respectively.

The interfacial area was changing with the reaction proceeding as iron and chromium were being dissolved in melt. The radius and immersion depth would contract simultaneously actually, which made the exact expression of the interfacial area impossible. In the analysis of Uslu et al. [27], the interfacial area was assumed to be a constant, which may cause errors. In this paper, the radius of the cylinder was fixed, while the immersion depth changed according to the weight of unreduced $FeCr_2O_4$. The radius of each $FeCr_2O_4$ cylinder was 1 cm and the weight of reduced $FeCr_2O_4$ was calculated from the alloyed chromium content in the sample metal. As a result, the interfacial area was calculated by equation (7).

$$A = 6.28 + 6.28\left(\frac{m_0 - m_{reduced}}{6.28\rho_m}\right) \tag{7}$$

where m_0, $m_{reduced}$ is the initial mass of the $FeCr_2O_4$ cylinder, the mass of the reduced $FeCr_2O_4$. The density of the melt was estimated as a function of the temperature and carbon concentration of the melt. The density of the melt was adopted from the investigation of Jimbo et al. [35], in which the density was expressed by $\rho_m = (7.10 - 0.073[\%C]) - (8.28 - 0.874[\%C])x10^{-4}(T - 182$, where the unit of temperature is Kelvin. Because it was assumed that the rate-controlling step was the CO formation reaction, the content of carbon at the interface was assumed to be equal to the carbon content in bulk melt. According to equation (6), the following equation can be derived:

$$4\frac{100M_C}{[C]A\rho_m} dn_{FeCr_2O_4} = k_r dt \tag{8}$$

where M_C and [C] is the mole mass of carbon and mass content of carbon of melt, respectively. Equation (9) can be obtained from the integration of both sides of equation (8).

$$4\int \frac{100M_C}{[C]A\rho_m} dn_{FeCr_2O_4} = \int k_r t dt \tag{9}$$

The left side of the equation (9) after integration is referred to as f(1) which is just an arbitrary notation, simply representing the value of the left side at different times. A plot of the left side of the equation (9) versus time should result in a straight line if the reduction of $FeCr_2O_4$ is controlled by the chemical reaction. The plots are presented in Fig. 9. It shows good linearity between f(1) and reaction time which indicates the reduction process was possibly controlled by interfacial chemical reaction. The reduction reaction rate coefficients were calculated by linear-regression analyses of the data.

It was found that the f(1) and time possessed good linearity in all experiments except the experiment at 1873 K. This good linearity implied that the CO formation chemical reaction was likely the rate-controlling step for the reduction of $FeCr_2O_4$ by

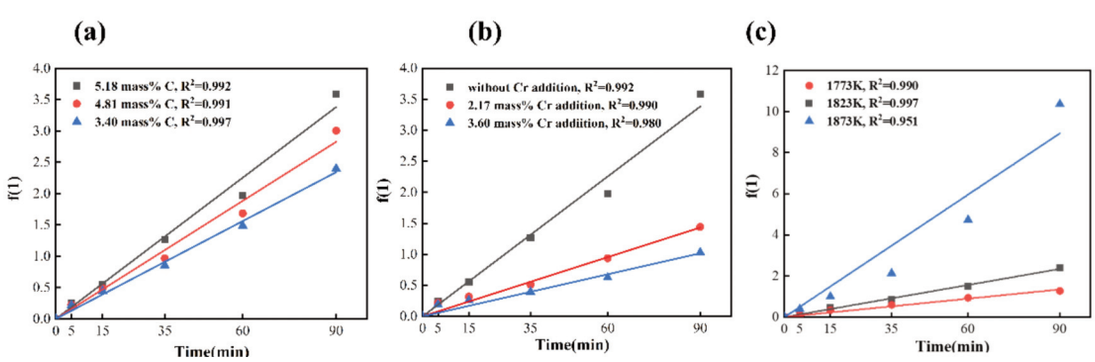

Figure 9. *The plot of the left-hand side of equation (11) as a function of time (a) with different initial carbon content, (b) with different chromium addition, and (c) at different temperatures*

carbon dissolved in iron melt through the experiment time except for the experiment at 1873 K.

3.2.2. Mass transport of oxygen

The evolution of the carbon monoxide near the $FeCr_2O_4$-melt boundary was considered to affect the $FeCr_2O_4$-melt and melt-gas area which accurate values were difficult to attain. However, in every experiment, most of the gas was observed to bubble in the vicinity of the cylinder-melt boundary. As a result, the mass transport of oxygen from the melt to the melt-gas boundary could be eliminated as the rate-determining step. Therefore, the mass transport of oxygen from the $FeCr_2O_4$-melt boundary to the melt was considered as follows:

$$-\frac{d[C]}{dt}=\left(\frac{M_C}{M_O}\right)\left(\frac{d[O]}{dt}\right)=\left(\frac{M_C}{M_O}\right)\left(\frac{A\rho_m}{W_m}\right)k_O([O_i]-[O_b]) \quad (10)$$

where the k_O is the mass transport coefficient of oxygen.

The $[O_i]$ and $[O_b]$ is the mass content of oxygen in the $FeCr_2O_4$-melt interface and melt, respectively. The subscript i denotes interface and b denotes bulk metal, the same in the latter. The $[O_b]$ can be obtained according to the equilibrium constant of equation (5):

$$k_1=\frac{P_{CO}}{a_{[O_b]}a_{[C_b]}}=\frac{P_{CO}}{f_{O_b}f_{C_b}[O_b][C_b]} \quad (11)$$

Where the f_{Ob} and f_{Cb} is the activity coefficient of oxygen and carbon in the melt. Their values can be evaluated from the first-order Wagner model as follows:

$$\lg f_{C_b}=e_C^C[C_b]+e_C^O[O_b]+e_C^{Cr}[Cr_b] \quad (12)$$

$$\lg f_{O_b}=e_O^C[C_b]+e_O^O[O_b]+e_O^{Cr}[Cr_b] \quad (13)$$

Combining the equation (11)-(13), the O_b can be obtained and thus the f_{Ob} can be obtained.

Similarly, the O_i can be obtained according to the equilibrium constant of equation (4):

$$k_2=a_{[Cr]}^2a_{[O_i]}^4a_{Fe}=(f_{[Cr]}[Cr])^2(f_{[O_i]}[O_i])^4a_{Fe} \quad (14)$$

Where the f_{Oi} and $f_{[Cr]}$ is the activity coefficient of oxygen and chromium in the cylinder/melt interface, respectively, and the is assumed to be one. The values of f_{Oi} and $f_{[Cr]}$ can be evaluated from the first-order Wagner model as follows:

$$\lg f_{C_i}=e_C^C[C_i]+e_C^O[O_i]+e_C^{Cr}[Cr_i] \quad (15)$$

$$\lg f_{O_i}=e_O^C[C_i]+e_O^O[O_i]+e_O^{Cr}[Cr_i] \quad (16)$$

As the mass transport of oxygen is assumed to be the rate-controlling step, the content of carbon and chromium in the cylinder/melt interface is assumed to be equal to that in the melt. Combining the equation (14)-(16), the can be obtained. Equation (17) can be obtained by the separation of variables and integration on both sides of equation (10).

$$-\left(\frac{M_O}{M_C}\right)\left(\frac{V_m}{A}\right)\int\frac{d[C]}{[O]_i-[O]_b}=\int k_O dt \quad (17)$$

Where the left side of the equation (17) after integration is referred to as f (2) which is just an arbitrary notation and simply represents the value of the left side at different times. A plot of the left side of the equation (17) versus time should result in a straight line if the reaction is transport-controlled, and if the mass-transfer coefficient of oxygen is constant. The value of f (2) vs time plot is presented in Fig.10.

It was found that, except in the experiment with chromium addition and experiment at 1773 K, the linearity between f (2) and time was poor when the oxygen transport from the interface to the melt was considered to be the rate-controlling step. The analysis of the rate-controlling step under different conditions will be discussed in the following section.

3.2.3. Summary of kinetic analysis

The R^2 which represents the linearity between f(1), f(2), and time under different experiment conditions are listed in Table 1. The f(1) is the left side of equation (9) when the CO formation reaction is considered to be the rate-controlling step for $FeCr_2O_4$ reduction. The f(2) is the left side of equation (17)

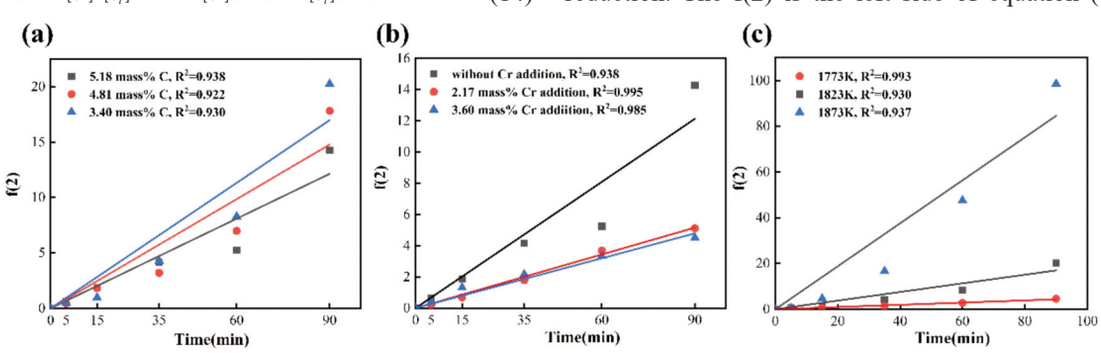

Figure 10. *The plot of the left-hand side of equation (17) as a function of time (a) with different initial carbon content, (b) with different chromium addition and (c) at different temperatures*

when the mass transport of oxygen from the cylinder/melt interface to the melt is considered to be the rate-controlling step for $FeCr_2O_4$ reduction.

Table 1. *The linearity between f(1), f(2), and time under different experiment condition (R^2)*

	5.18 wt% C	4.81 wt% C	3.40 wt% C	2.17 wt% Cr	3.60 wt% Cr	1773K	1823K
f(1)	0.992	0.991	0.997	0.990	0.980	0.990	0.951
f(2)	0.938	0.922	0.930	0.995	0.985	0.993	0.937

It was found that the R^2 of f(1) and t was higher than that of f(2) and t without chromium addition at 1823 K. This implied that the CO formation reaction was more likely to be the rate-controlling step under these three experimental conditions. The R^2 of f(2) and t was near to that of f(1) and t when the chromium was added to the iron melt at the beginning and when the experiment was conducted at 1773 K. As chromium was added to the melt, the residual carbon content in the melt increased. As a result, the oxygen solubility in the melt had a tendency to decrease. Therefore, the driving force for the mass transport of oxygen decreased. As a result, the mass transport of oxygen was more like to be the rate-controlling step under these conditions. Similarly, USLU et al. [27] concluded that the mass transport of oxygen from the chromite/melt interface to the melt was a rate-controlling step when the chromium content in the iron melt was around 47-57 wt%. The mass transport coefficient of oxygen in the experiment with 2.17 wt% and 3.60 wt% Cr addition was $9.55e^{-4}$ and $8.87e^{-4}$ cm/s. The calculated mass transport coefficient of oxygen was in the same order as the results of Ding et al. [25].

It is well known that temperature is the important factor affecting the reaction rate. The experiment when the initial carbon content was 3.40 wt% at 1823 K was considered to be controlled by the CO formation reaction. As a result, the experiment with the same initial carbon content at 1823 K was also considered to be controlled by the CO formation reaction.

When the experiment temperature was 1873 K, the R^2 of both assumptions was relatively small when it was fitted through the whole experiment time. However, good linearity was found between f(1) and t in the first 35 min and good linearity was found between f(2) and t after 35 min, as shown in Fig.11. As a result, at 1873 K, the reduction of $FeCr_2O_4$ was likely to be controlled by the CO formation reaction in the first 35 min. The mass transport of oxygen was likely to be the rate-controlling step when the reaction proceeded after 35 min.

Based on the above analysis, the chemical reaction rate constant of CO formation could be calculated as shown in Fig.12. The reaction rate constant increased with increasing initial carbon content and temperature. When the temperature increased from 1823 to 1873 K, the rate constant increased more substantially than the increment from 1773 to 1823 K. Similarly, when the temperature increased from 4.81 wt% to 5.18 wt%, the rate constant increased substantially. As a result, the temperature for reduction of $FeCr_2O_4$ by carbon dissolving in the iron melt was suggested to be higher than 1823 K.

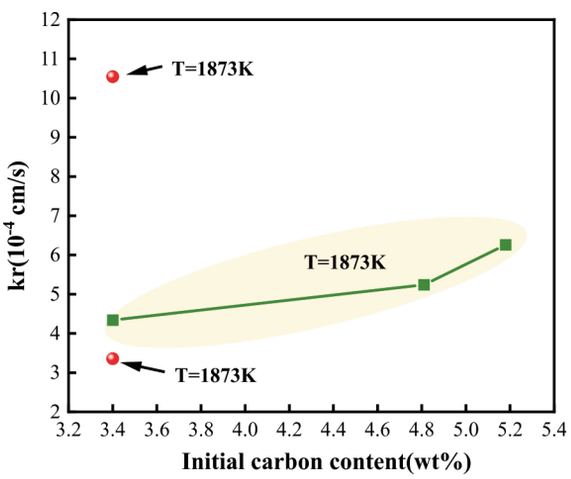

Figure 12. *Rate constant k_r under different conditions*

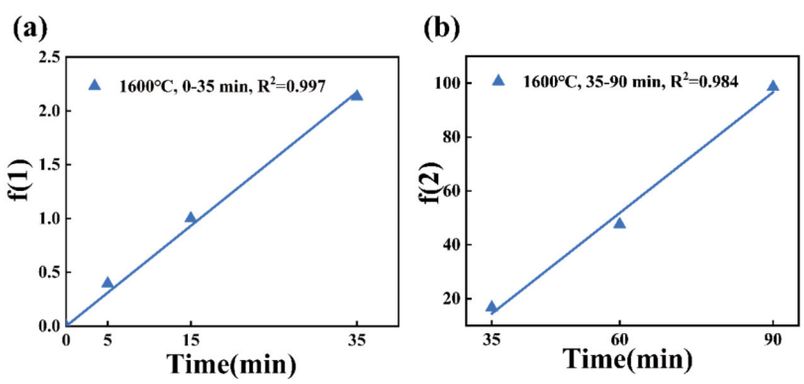

Figure 11. *f(1) as a function of time in (a) 0-35 min and (b) 35-90 min at 1873K*

The activation energy of the CO formation reaction can be calculated for the experiment without Cr addition according to the Arrhenius formula as equation (18).

$$k_r = A\exp(-E_a / R)\frac{1}{T} \quad (18)$$

Equation (18) can be deduced according to equation (19).

$$\ln k_r = \ln A + (\frac{-E_a}{R})\frac{1}{T} \quad (19)$$

As a result, the activation energy Ea can be obtained from the slope of the linearity between $\ln k_r$ and 1/T as shown in Fig. 13. The calculated activation energy for the reaction was 392.82 kJ/mol which was relatively large [36]. The large activation energy was consistent with the former conclusion that the rate-controlling step for the reduction of $FeCr_2O_4$ by carbon dissolving in the iron-baes melt was the interfacial reaction.

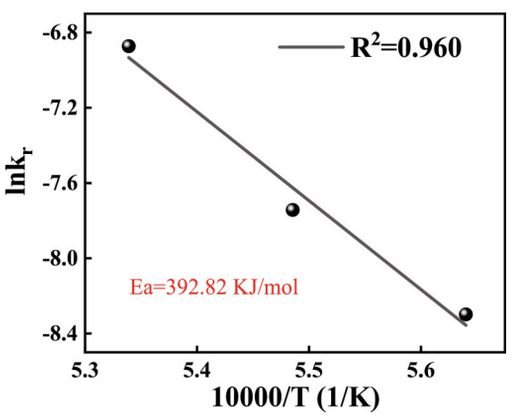

Figure 13. *Plot of rate constant k_r as a function of temperature for reduction of $FeCr_2O_4$ by carbon dissolving in the iron melt*

4. Conclusion

The reduction of synthetic $FeCr_2O_4$ by carbon dissolved in the iron melt was conducted. The reduction extent of $FeCr_2O_4$ was detected by the measurement of the composition of the alloy. The result of the experiments showed that the $FeCr_2O_4$ was successfully reduced to chromium alloying in the iron melt. The research results can be summarized as follows:

The chromium recovery increased with increasing initial carbon content. Similarly, the higher temperature was favorable to the reduction of $FeCr_2O_4$. 89.85 mass% of $FeCr_2O_4$ was reduced at 1873 K after 90 min when the initial carbon content was 3.40 mass% without the addition of chromium. In the meantime, the chromium content in the melt reached 5.56 mass%.

The effect of chromium addition on the reduction of $FeCr_2O_4$ by carbon dissolving in the melt was studied. The negative effect of chromium originated from the strong attraction between chromium and carbon which resulted in a decrease in carbon activity.

The controlling step for the $FeCr_2O_4$ reduction by carbon dissolving in the iron melt without Cr addition was the chemical reaction in the whole 90 min when the temperature was 1773 K and 1823 K. At 1873 K, the chemical reaction at $FeCr_2O_4$/melt interface was the rate-controlling step in the first 35 min. While after 35 min, the rate-controlling step became the mass transfer of oxygen from the $FeCr_2O_4$/melt interface to the iron melt. The activation energy for the chemical reaction was 392.82 kJ/mol.

Acknowledgement

The authors are grateful for the financial support of this work from the National Natural Science Foundation of China (No. 51922003, 52274406) and Fundamental Research Funds for the Central Universities (No. FRF-TP-19-004C1, FRF-BD-22-04).

Author contributions

Pro. L.-J. Wang conducted the supervision and project administration. Y.-Y Xiao performed the original draft writing and leaded the formal analysis. S.-Y. Liu and X.-B. He conducted the writing-reviewing and editing. K.-C. Chou conducted the writing-reviewing, too.

Data availability

The data of this work could be obtained by contacting with the corresponding author by e-mail.

Conflict of interest

On behalf of all authors, the corresponding author states that there is no conflict of interest.

Reference

[1] X.F. Hu, L.S. Okvist, J. Eriksson, Q.X. Yang, B. Bjorkman, Direct alloying steel with chromium by briquettes made from chromite ore, mill scale, and petroleum coke, Steel Research International, 88 (5) (2017) 1-10. https://dx.doi.org/10.1002/srin.201600247

[2] P.H. Kumar, A. Srivastava, V. Kumar, M.R. Majhi, V.K. Singh, Implementation of industrial waste ferrochrome slag in conventional and low cement castables: Effect of microsilica addition, Journal of Asian Ceramic Societies, 2 (2) (2014) 169-175. https://doi.org/10.1016/j.jascer.2014.03.004

[3] J. Johnson, L. Schewel, T.E. Graedel, The

Contemporary Anthropogenic Chromium Cycle, Environmental Science & Technology, 40 (2006) 7060-7069. https://dx.doi.org/10.1021/es060061i

[4] S. Liu, L. Ye, L. Wang, K.-C. Chou, Selective oxidation of vanadium from vanadium slag by CO2 during CaCO3 roasting treatment, Separation and Purification Technology, 312 (2023) 123407-123416. https://doi.org/10.1016/j.seppur.2023.123407

[5] Q. Zeng, J.L. Li, G.J. Ma, H.Y. Zhu, Effect of binary basicity on chromium occurrence in stainless steel slag, Journal of Mining and Metallurgy, Section B: Metallurgy, 58 (1) (2022) 11-18. https://doi.org/10.2298/jmmb210304043z

[6] A. Ahmed, M.K. El-Fawakhry, M. Eissa, S. Shahein, Direct chromium alloying by smelting reduction of mill scale and low grade chromite ore, Ironmaking & Steelmaking, 42 (9) (2015) 648-655. https://dx.doi.org/10.1179/1743281215y.0000000008

[7] O.D. Brovko, Y.A. Bublikov, I.V. Mezhebovskii, S.N. Podgornyi, G.A. Polyakov, A.S. Popov, A.V. Rabinovich, Y.V. Sadovnik, Direct chromium alloying of steel using poor chromium-containing raw materials, Russian Metallurgy (Metally), 2013 (12) (2014) 952-956. https://dx.doi.org/10.1134/s0036029513120045

[8] Y. Kishimoto, K. Taoka, S. Takeuchi, Rolling Technology and Modernization of Chiba Works 1997.

[9] N.Z. Mukashev, N.Y. Kosdauletov, B.T. Suleimen, Comparison of iron and chromium reduction from chrome ore concentrates by solid carbon and carbon monoxide, Solid State Phenomena, 299 (2020) 1152-1157. https://dx.doi.org/10.4028/www.scientific.net/SSP.299.1152

[10] Q.C. Yu, Y. Deng, S.B. Yin, Z.Y. Li, Thermal process for magnesium production with Al-Si-Fe from coal fly ash: Thermodynamics and experimental investigation, Journal of Mining and Metallurgy, Section B: Metallurgy, 57 (3) (2021) 421-430. https://doi.org/10.2298/jmmb210118038y

[11] S. Eray, E. Keskinkilic, Y.A. Topkaya, A. Geveci, Reduction behavior of iron in the red mud, Journal of Mining and Metallurgy, Section B: Metallurgy, 57 (3) (2021) 431-437. https://doi.org/10.2298/jmmb210227039e

[12] F.G. Lei, M.T. Li, C. Wei, Z.G. Deng, X.B. Li, G. Fan, Recovery of zinc from zinc oxide dust containing multiple metal elements by carbothermal reduction, Journal of Mining and Metallurgy, Section B: Metallurgy, 58 (1) (2022) 85-96. https://doi.org/10.2298/jmmb2011020491

[13] X.F. Hu, L.S. O¨kvist, Q.X. Yang, B. Bjo¨rkman, Thermogravimetric study on carbothermic reduction of chromite ore under non isothermal conditions, Ironmaking & Steelmaking, 42 (6) (2015) 409-416. https://doi.org/10.1179/1743281214Y.0000000243

[14] Y.X. Wang, L.J. Wang, J. Yu, K.C. Chou, Kinetics of carbothermic reduction of synthetic chromite, Jornal of Mining and Metallurgy,Section B:Metallurgy, 50 (1) (2014) 15-21. https://dx.doi.org/10.2298/JMMB130125008W

[15] D. Chakraborty, S. Ranganathan, S.N. Sinha, Investigations on the carbothermic reduction of chromite rres, Metallurgical and Materials Transactions B, 36B (2005) 437-444. https://doi.org/10.1007/s11663-005-0034-z

[16] O. Soykan, R.H. Eric, R.P. King, Kinetics of the reduction of bushveld complex chromite ore at 1416 °C, Metallurgical and Materials Transactions B, 22B (1991) https://doi.org/10.1007/BF02651157

[17] K.P.D. Perry, C.W.P. Finn, R.P. King, An ionic diffusion mechanism of chromite reduction, Metallurgical and Materials Transaction B, 19 (4) (1988) 677-684. https://dx.doi.org/10.1007/bf02659161

[18] X.F. Hu, H. Wang, L. Teng, S. Seetharaman, Direct chromium alloying by chromite ore with the presence of metallic iron, Journal of Mining and Metallurgy, Section B: Metallurgy, 49 (2) (2013) 207-215. https://doi.org/10.2298/jmmb120815015h

[19] X.F. Hu, Q.X. Yang, L.S. Okvist, B. Bjorkman, Thermal analysis study on the carbothermic reduction of chromite ore with the addition of mill scale, Steel Reasearch International, 87 (5) (2016) 562-570. https://dx.doi.org/10.1002/srin.201500131

[20] X.F. Hu, L.D. Teng, H.J. Wang, L.S. Okvist, Q.X. Yang, B. Bjorkman, S. Seetharaman, Carbothermic reduction of synthetic chromite with/without the addition of iron powder, ISIJ International, 56 (12) (2016) 2147-2155. https://dx.doi.org/10.2355/isijinternational.ISIJINT-2016-337

[21] Y. Liu, M.F. jiang, L.X. Xu, D.Y. Wang, Mathematical Modeling of Refining of Stainless Steel in Smelting Reduction Converter Using Chromium Ore, ISIJ International, 52 (3) (2012) 394-402. https://dx.doi.org/10.2355/ISIJINTERNATIONAL.52.394

[22] Y. Liu, M.F. Jiang, D.Y. Wang, L.X. Xu, Dissolution kinetics of chromium ore in slag system for stainless steelmaking, Canadian Metallurgical Quarterly, 51 (1) (2012) 24-30. https://dx.doi.org/10.1179/1879139511y.0000000017

[23] M.B.C. Tsomondo, D.J. Simbi, Kinetics of chromite ore reduction from MgO-CaO-SiO2-FeO-Cr2O3-Al2O3slag system by carbon dissolved in high carbon ferrochromium alloy bath, Ironmaking & Steelmaking, 29 (1) (2002) 22-28. https://doi.org/10.1179/030192302225001956

[24] D.J. Simbi, M.B.C. Tsomondo, Aspects of smelting reduction of chromite ore fines in CaO-FeO-Cr2O3-SiO2-Al2O3slag system by carbon dissolved in high carbon ferrochromium alloy bath, Ironmaking & Steelmaking, 29 (4) (2013) 271-275. https://doi.org/10.1179/030192302225004520

[25] Y.L. Ding, A.J. Merchant, Kinetics and mechanism of smelting reduction of fluxed chromite Part 2 Chromite–flux pellets in Fe–C–Si melts, Ironmaking & Steelmaking, 26 (4) (1999) 254-261. https://doi.org/10.1179/030192399677112

[26] Y.L. Ding, A.J. Merchant, Kinetics and mechanism of smelting reduction of fluxed chromite part1 Carbon-chromite-flux composite pellets in Fe-Cr-C-Si melts, Ironmaking & Steelmaking, 26 (4) (1999) 247-253. https://doi.org/10.1179/030192399677103

[27] E. Uslu, R.H. Eric, The reduction of chromite in liquid iron-chromium-carbon alloys, Journal of the Southern African Institute of Mining and Metallurgy, 91 (11) (1991) 397-409. https://dx.doi.org/10.10520/AJA0038223X_2081

[28] O. Demir, R.H. Eric, Reduction of Chromite in Liquid Fe-Cr-C-Si Alloys, Metallurgical and Materials Transaction B, 25B (1994) 549-559.

https://doi.org/10.1007/BF02650075

[29] J.W. Matousek, Henry's Law Activity of Oxygen in Molten Iron, JOM, 67 (9) (2015) 1933-1935. https://dx.doi.org/10.1007/s11837-015-1485-6

[30] L. Yang, M.T. Simnad, G. Derge, The diffusion of carbon in iron-carbon alloys at 1560°C, Journal of Metals, (1956) 1643-1648. https://doi.org/10.1007/BF02646337

[31] R.J. Fruehan, Rate of reduction of Cr2O3 by carbon and carbon dissolved in liquid iron alloys, Metallurgical and Materials Transaction B, 8B (1977) (1977) 429-433. https://doi.org/10.1007/BF02696929

[32] E. Shibata, H. Sun, K. Mori, Kinetics of reaction between MnO based slag and Fe-C-P-Si alloy, Tetsu-To-Hagane, 82 (7) (1996) 575-580. https://dx.doi.org/10.2355/tetsutohagane1955.82.7_575

[33] E. Shibata, H. Sun, K. Mori, Kinetics of simultaneous reactions between liquid iron-carbon alloys and slags containing MnO, Metaluurgical and Materials Transaction B, 30B (1999) (1999) 279-286.https://doi.org/10.1007/s11663-999-0057-y

[34] T. Nakasuga, K. Nakashima, K. Mori, Recovery rate of chromium from stainless slag by iron melts, ISIJ International, 44 (4) (2004) 665-672. https://doi.org/10.2355/isijinternational.44.665

[35] I. Jimbo, A.W. Cramb, The density of liquid iron-carbon alloys, Metallurgical and Materials Transaction B, 24 (1) (1993) 5-10. https://dx.doi.org/10.1007/bf02657866

[36] T. Nakasuga, H. Sun, K. Nakashima, K. Mori, Reduction rate of Cr2O3 in a solid powder state and in CaO-SiO2-Al2O3-CaF2 slags by Fe-C-Si melts, ISIJ International, 41 (9) (2001) 937-944. https://dx.doi.org/10.2355/isijinternational.41.937

KINETIČKI MEHANIZAM TOKOM REDUKCIJE $FeCr_2O_4$ U RASTOPU GVOŽĐA KOJI SADRŽI UGLJENIK

Y.-Y. Xiao [a], L.-J. Wang [a,*], S.-Y. Liu [a], X.-B. He [a], K.-C. Chou [b]

[a] Centar za kolaborativnu inovaciju u tehnologiji čelika (CICST), Univerzitet za nauku i tehnologiju u Pekingu, Peking, Kina

[b] Glavna državna laboratorija za naprednu metalurgiju, Univerzitet za nauku i tehnologiju u Pekingu, Peking, Kina

Apstrakt

Direktno legiranje hroma hromitom privlači veliku pažnju zbog svoje superiornosti u uštedi i pojednostavljenosti procesa. Poznavanje postupka legiranja hroma redukcijom $FeCr_2O_4$, koji je glavni sastojak hromita, ključno je za razumevanje mehanizma legiranja hroma na ovaj način. Ispitan je uticaj sastava rastopa (sa dodatkom ugljenika i hroma) i temperature na redukciju $FeCr_2O_4$ u rastopu gvožđa koji sadrži ugljenik. Sa većim sadržajem ugljenika u rastopu, više hroma je dobijeno. Slično tome, viša temperatura je pogodovala redukciji $FeCr_2O_4$. Dodatak hroma je ometao redukciju $FeCr_2O_4$ zbog niže aktivnosti ugljenika koja proizilazi iz jakog privlačenje između ugljenika i hroma. Ispitivana je i kinetika redukcije $FeCr_2O_4$ u rastopu gvožđa sa sadržajem ugljenika, a rezultati su pokazali da je kontrolni korak bila hemijska reakcija na granici $FeCr_2O_4$/rastop na 1823 K. Izračunata aktivaciona energija za ovu hemijsku reakciju bila je 392,82 kJ/mol.

Ključne reči: *Legiranje hroma; Ruda hromit; $FeCr_2O_4$; Nerđajući čelik*